Basic topology of twisted magnetic configurations in solar flares

Article *in* Astronomy and Astrophysics · October 1999

CITATIONS
136

READS
65

2 authors:

Viacheslav S. Titov
Predictive Science Inc.
144 PUBLICATIONS **2,818** CITATIONS
SEE PROFILE

Pascal Demoulin
Observatoire de Paris
404 PUBLICATIONS **8,132** CITATIONS
SEE PROFILE

Astron. Astrophys. 351, 707–720 (1999)

ASTRONOMY AND ASTROPHYSICS

Basic topology of twisted magnetic configurations in solar flares

V.S. Titov[1] **and P. Démoulin**[2]

[1] Theoretische Physik IV, Ruhr-Universität Bochum, 44780 Bochum, Germany (st@tp4.ruhr-uni-bochum.de)
[2] DASOP, Observatoire de Paris-Meudon, 92195 Meudon cedex, France (demoulin@obspm.fr)

Received 17 May 1999 / Accepted 9 July 1999

Abstract. It is accepted now that flare-like phenomena are the result of reconnection of topologically complex magnetic fields. Observations show that such fields are often characterized by a twisted structure. This is modeled here using a force-free flux tube whose arc-like body is embedded into an external potential magnetic field. We study how the topological structure of this configuration evolves when the flux tube emerges quasi-statically from below the photosphere to a certain height in the corona, where the tube becomes unstable and its eruption has to occur. During this evolution below the flux tube there appears a separator field line, along which two separatrix surfaces intersect. This separator is of generalized type because there are no magnetic nulls in the configuration. Both the separator and the separatrices are topological features, where the connectivity of magnetic field lines suffers a jump. We propose that the eruption of the flux tube has to stimulate the formation of strong current layers, in which the free magnetic energy of configuration is released in the form of a flare. The model predicts the formation of hot loops of two kinds during the reconnection phase: the long loops which make nearly one turn around the twisted flux tube, and short sheared loops below. The proposed model provides important clues to the mechanism of solar flares in twisted configurations.

Key words: Sun: flares – Sun: magnetic fields – Sun: prominences – Sun: X-rays, gamma rays

1. Introduction

The magnetic field under typical coronal conditions is force-free and well frozen into plasma almost everywhere in active regions on the Sun. An exception is separatrix surfaces or separatrices, where the plasmo-magnetic system behaves in a different way such that the current layers with a strong resistive dissipation inside may be formed. This fact is very important for understanding effective mechanisms of magnetic energy release in a highly conductive coronal plasma.

It has been known for a long time (cf. the reviews of Syrovatskii (1981) and van den Oord (1993)) that in 2D magnetic configurations the formation of current sheets occurs in the neighbourhood of neutral X-points. Adding a third perpendicular component of the field, which is invariant in this perpendicular direction (so-called $2\frac{1}{2}$D configurations), yields a new possibility for the current sheet formation. They can be formed now along the separatrices during a quasi-static evolution driven by smooth shearing flows at the photospheric boundary, where the frozen-in and line-tying conditions are supposed to be fulfilled (Zwingmann et al. 1985). This may occur not only when the separatrices are due to the presence of an X-point in the poloidal field (Low & Wolfson 1988; Finn & Lau 1991; Vekstein & Priest 1992), but also when they are conditioned by the field lines, which are tangent to the photospheric boundary (Low 1987; Aly & Amari 1989; Wolfson 1989; Vekstein et al. 1991; Low 1992).

Numerical simulations of time-dependent MHD equations for the photospheric line-tying conditions (Karpen et al. 1990, 1991) confirmed the formation of quasi-static current sheets near separatrices. However, their simulations for other boundary conditions modelling gravitationally stratified photosphere showed that, instead of such sheets, current layers of finite thickness are formed. For this reason Karpen et al.(1991) argued that the magnetic field is attached to the photosphere only on a photospheric gravitational scale height and so the corresponding thickness of current layers is not small enough for switching an essential resistive dissipation on. Billinghurst et al.(1993) showed, however, that if the field strength decreases sufficiently rapidly towards the place of field line contact with the photosphere, the current layers in corona may still be thin enough for this dissipation to be important.

In 3D generic cases the separatrices consist of the field lines, which either thread magnetic nulls or touch special segments of the photospheric inversion line (see e.g. Seehafer 1986). For the second case, due to a characteristic concave pattern of the field lines near these segments, we call them bald patches or briefly BPs (Titov et al.1993). These separatrices are thought to be the surfaces, along which the current sheets are formed in the course of quasi-static evolution driven by slow photospheric flows of plasma (e.g. Aly 1990, Lau 1993). The present observations, however, do not indicate a systematic relation of magnetic nulls with flares (Démoulin et al.1994). On the other hand, there is some evidence for the role of BPs in flares. The first examples were given implicitly by Seehafer & Staude (1980) and Seehafer

Send offprint requests to: V.S. Titov

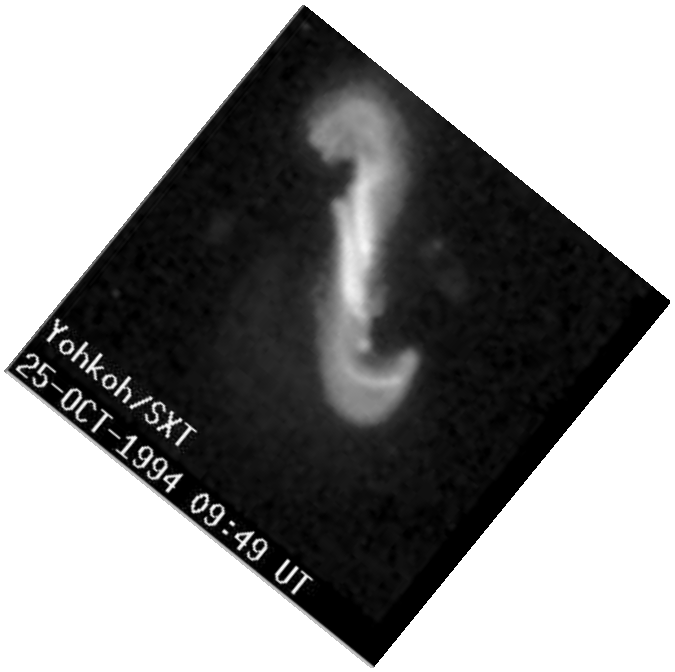

Fig. 1. A typical structure of X-ray loops observed on the disk in solar flares with a twisted magnetic field (Courtesy L. van Driel-Gesztelyi).

(1985) (the complex topology obtained is now recognized as due to the presence of BPs: see Seehafer 1986). More recently, Aulanier et al.(1998b) found a close correspondence between the BP separatrices and the Hα and soft X-ray emission in a small flare.

One can see from this discussion that it is worth analyzing the presence of BPs in magnetic configurations modelling active regions (ARs) on the Sun. This was first done in general form by Seehafer (1986), and later Titov et al.(1993) essentially detailed this in the example of configurations formed by four photospheric field sources with one main and one parasitic bipoles. They showed that in both potential and linear force-free approximations, a BP exists at the center of the configuration for a wide range of parameters. Bungey et al.(1996) studied the splitting or bifurcation of such a BP when the parasitic bipole is increasing its strength. This bifurcation of BP gives birth to a separator field line in the form of an intersection of two separatrices associated with each bifurcated part. That was the first known example of a separator which is not caused by the presence of two magnetic null points in the coronal field.

The aim of this paper is to extend previous studies on BPs to configurations with nonlinear force-free magnetic fields. There is much observational evidence for strong magnetic shear in solar eruptions indicating that these phenomena are connected with such magnetic fields. Helical-like magnetic structures are typically ejected into interplanetary space during eruptions of prominences, as is frequently suggested by Hα observations on the disk (e.g. Raadu et al.1988) and even more often on the limb (e.g. Rompolt 1990, Vršnak et al.1991). Similarly, in soft X-ray range the Yohkoh satellite also provides examples of S-shaped coronal loops (see, e.g., Pevtsov et al.1996, Rust and Kumar 1994 and Manoharan et al.1996, and Fig. 1), which are interpreted as a signature of erupting twisted configurations associated with filament and coronal mass ejections.

In this article we assume that the basic topology of such configurations can be modeled by using a simple model, in which an arc-like body of the twisted force-free tube is embedded into a potential background field. The advantage of this model (proposed earlier by Titov & Démoulin (1999)) is that the equilibrium parameters of a twisted flux tube as well as the magnetic field itself can be found analytically (Sect. 2). After this the conditions of the presence of BPs in the modelling magnetic field are analyzed in Sect. 3. Then the global magnetic topology caused by these local topological features is studied in Sect. 4. An emphasis is made on the cases when the above mentioned generalized separator is present. In Sect. 5 this topological structure is compared with a similar one found previously for a purely potential field by Bungey et al. (1996). Then we consider a relationship between the distribution of electric current and magnetic topology in Sect. 6. The relevance of BPs for defining the location of energy release in coronal magnetic configurations is summarized in Sect. 7.

2. A simple model for twisted configurations

2.1. General construction of the model and equilibrium condition

In active regions on the Sun the following physical conditions are usually fulfilled. First, the characteristic time of propagation of Alfvén waves through the whole region is much less than the corresponding time of the global evolution of the region, so that the dynamical or inertia effect is negligible. Secondly, the pressure and weight of plasma are also negligible in comparison with magnetic pressure and tension, which therefore counterbalance each other and so yield approximately vanishing Lorentz force $\boldsymbol{j} \times \boldsymbol{B}$. Altogether, this means that the system evolves through a sequence of force-free equilibria satisfying

$$\boldsymbol{j} \times \boldsymbol{B} \;=\; 0\,, \tag{1}$$

$$\boldsymbol{j} \;=\; \mu_0^{-1}\, \boldsymbol{\nabla} \times \boldsymbol{B}\,, \tag{2}$$

$$\boldsymbol{\nabla} \cdot \boldsymbol{B} \;=\; 0\,. \tag{3}$$

These equations are usually complemented by the corresponding boundary conditions at the photosphere and vanishing asymptotics of the magnetic field $\boldsymbol{B}$ at infinity.

Generally, it is very difficult to solve such a problem in realistically meaningful cases. However, our prime interest here concerns the topology of magnetic field and this makes it possible to simplify the problem to an analytically treatable form. Indeed, the magnetic topology is derived from the field line integration, where the field in turn is a result of the appropriate integration over the current distribution. Such a double integration averages local variations of the current density and thereby makes the magnetic topology insensible to these variations (an additional reason for the magnetic topology to be robust is described in Sect. 3). This is confirmed by many concrete examples, which show that the topology depends mainly

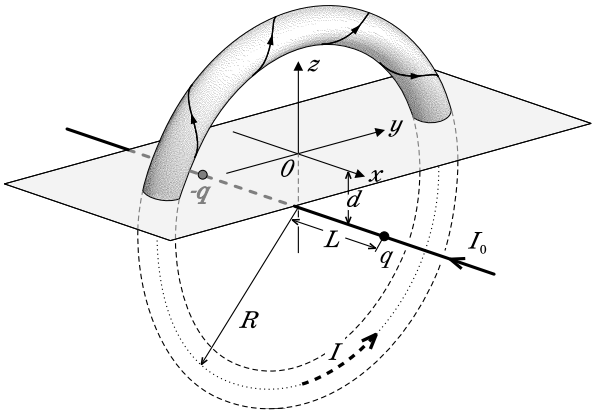

Fig. 2. The magnetic field under study is modeled by a force-free circular flux tube with the total current I, a pair of magnetic charges $-q$, q and a line current I_0. Below the photospheric plane $z = 0$ this configuration has no real physical meaning: it is used only to construct the proper magnetic field in corona.

on the large-scale features of the current distribution. So we probably do not lose too much in understanding the topology of a generic twisted configuration if one concentrates all the current within an arc-like loop of a force-free tube embedded into a potential magnetic field.

To construct this configuration, let us introduce a Cartesian system of coordinates in which the z-axis points in the vertical direction and the plane $z = 0$ represents the photosphere (Fig. 2). The whole magnetic field is obtained here by superimposing three components denoted by $\boldsymbol{B}_I$, $\boldsymbol{B}_q$ and $\boldsymbol{B}_\theta$. The first component $\boldsymbol{B}_I$ is the field created by a ring current I uniformly distributed over its circular cross section of radius a. The plane of symmetry of the ring coincides with the plane $x = 0$, while its axis of symmetry is parallel to the x-axis and submerged under the photosphere by a depth d, so that in corona only an arc of the ring with major radius R is present. The second component $\boldsymbol{B}_q$ is created by the leading and following spots of the modeling active region, which are represented here by two charges $-q$ and q lying on the axis of symmetry of the ring from both sides of the plane $x = 0$ on the distance L. The third component $\boldsymbol{B}_\theta$ is created by a line current I_0 flowing exactly along the axis of symmetry of the ring. In this model, of course, only the field above the photospheric plane $z = 0$ has a real physical meaning, while the sub-photospheric currents and sources play an auxiliary role in constructing the configuration. One can ignore its sub-photospheric part and regard that the coronal force-free field is in fact determined by the vertical components of the field $\boldsymbol{B}_q + \boldsymbol{B}_I + \boldsymbol{B}_\theta$ and current density on the photosphere (only in one polarity for the current).

The region occupied by the ring current is further assumed to be thin, so that the equilibrium of this current can be investigated by using appropriate asymptotic expansions in small parameters a/R and a/L. In zero order approximation, this problem reduced to a force free condition in the cross section of the flux tube – which we will futher call the "internal equilibrium". In the next order, it reduces to an equilibrium condition for each current element of the tube in the magnetic field created by external sources and the rest current elements – which we will call the "external equilibrium". Such a decomposition of the equilibrium problem is true both in purely 2D case (Isenberg et al.1993) and in more general 3D case (Lin et al. 1998). The internal equilibrium is very simple in our case, since it just coincides with a force free equilibrium of a straight flux tube having a circular cross section. The corresponding solution is well known and, in particular, it allows the possibility assumed here that the toroidal current density is uniformly distributed in the cross section of the flux tube. The details of how these internal and external solutions can be sewed are described in Sect. 2.2.

The external equilibrium here corresponds to the equilibrium of a ring current in an axisymmetric potential field. Due to the present axial symmetry, the respective equilibrium condition is the same for each element of the flux tube and, is reduced to the balance of only two forces: the Lorentz force $\boldsymbol{F}_q$ caused by interaction of the current I with the field $\boldsymbol{B}_q$ and the Lorentz self-force $\boldsymbol{F}_I$ resulting from the curvature of the tube axis. Both forces act along the normal $\boldsymbol{n}$ to this axis and can be written as

$$\boldsymbol{F}_q = -\frac{2qLI\boldsymbol{n}}{(R^2+L^2)^{3/2}}\,, \tag{4}$$

$$\boldsymbol{F}_I = \frac{\mu_0 I^2}{4\pi R}\left(\ln\frac{R}{a} + \ln 8 - 3/2 + l_\mathrm{i}/2\right)\boldsymbol{n}\,, \tag{5}$$

where l_i is the internal self-inductance per unit length of the tube (Shafranov 1966). It is always of the order of unity and so the contribution of l_i is smaller than $\ln(R/a)$ at $R/a \gtrsim 1$. For example, $l_\mathrm{i} = 1/2$ in our case of the uniform distribution of toroidal current in the flux tube. We shall further retain this current distribution with such an l_i, realizing that its variation must yield nearly the same results.

From the force balance $\boldsymbol{F}_q + \boldsymbol{F}_I = 0$ we obtain the total equilibrium current

$$I = \frac{8\pi qLR(R^2+L^2)^{-3/2}}{\mu_0\left[\ln(8R/a) - 3/2 + l_\mathrm{i}/2\right]}\,, \tag{6}$$

which flows in the corona. The toroidal field component $\boldsymbol{B}_\theta$ does not participate here explicitly, but its presence provides an internal force-free equilibrium of the flux tube. One can expect that the greater the value of B_θ, the more stable the equilibrium of the tube is (in particular with respect to kink mode instability). Also the above mentioned robustness of the magnetic topology to spatial variations of the current density enables us to ignore the corrections of higher orders (proportional to $(a/R)^2$ and a/L) to the magnetic field under study.

Suppose now that the modeling configuration is formed due to an emergence from the photosphere of the flux tube with gradually increasing R. This corresponds to typically observed diverging movements of two magnetic polarities represented in our model by the photospheric intersections of the flux tube. In particular, such a scenario is suggested by recent measurements of magnetic field vectors (Leka et al.1996; Lites et al.1995). Suppose that the flux tube under the photosphere is twisted more

slowly than it emerges in the corona (owing to the effect of buoyancy). This assumption would correspond in our model to a constant number N_t of field-line turns in the torus. Since the windings are uniformly distributed along the torus, the number $N_{\rm cor}$ of field-line turns along its coronal part increases with R as

$$N_{\rm cor} \approx \frac{N_t}{\pi} \arccos \frac{d}{R}\,, \tag{7}$$

where N_t can be expressed in terms of I and B_θ as follows. Note first that the observed values of $N_{\rm cor}$ in twisted configurations never exceed several units – this fact in combination with the inequality $a \ll R$ means that the toroidal component is much larger than the poloidal one and so B_θ inside the tube is approximately the same as in its vicinity. Thus this component is nearly uniform at the flux tube and described by

$$B_\theta \approx \frac{\mu_0 I_0}{2\pi R}\,, \tag{8}$$

where I_0 is also assumed to be constant during the emergence of the tube. By taking into account now the approximate homogeneity of B_θ we obtain

$$N_t \approx \frac{\mu_0 I R}{2\pi a^2 |B_\theta|}\,, \tag{9}$$

where the current I and the field B_θ are supposed to evolve with increasing R in accordance with Eqs. (6) and (8), respectively. From here and from the constancy assumed above of N_t, one can determine the corresponding evolution of the tube radius a in terms of solutions of the following transcendental equation:

$$\frac{a}{L} \approx 2 \left\{ \frac{2\pi q\,(R/L)^3\,[(R/L)^2+1]^{-3/2}}{\mu_0 N_t |I_0| L\,[\ln(8R/a) - 3/2 + l_{\rm i}/2]} \right\}^{1/2}. \tag{10}$$

Here the logarithmic term $\ln(R/a)$ can be considered in the first approximation as a constant, so that $a \sim R^{3/2}$ at small R and a saturates at some level when $R \gtrsim L$.

During such a quasi-static emergence of the flux tube, its equilibrium can become unstable at some R, for which a small displacement of the tube, represented here by δR, will cause a perturbation δF_I larger than δF_q (as it similarly happens in 2D models, see Isenberg et al.1993; Forbes and Priest 1995, and references therein). The simplest indication on this is seen from the dependence of current I on radius R given by Eq. 6, where I has a maximum at $R \equiv R_{I_{\max}} \approx L/\sqrt{2}$. The instability at $R_{I_{\max}}$, however, is not realized, since in reality the photospheric line-tying preserves $N_{\rm cor}$, which yields a stabilizing effect for the whole system and shifts the onset of the instability to larger values of radius as shown in Fig. 3 ($R \approx L\sqrt{2}$, for details see Appendix and Lin et al.1998).

Thus, each equilibrium here is characterized by six free parameters R, N_t, q, L, I_0 and d. Their possible variation will be reduced in this work to a few cases illustrating the model in the range where the instability is likely to happen. The various magnetic topologies are presented in this model with a plausible scenario of the flux tube emergence, in which the intensity and positions of the sub-photospheric sources (q, L, I_0 and d) remain constant and the emergence occurs without twisting motions ($N_t = \text{const} \sim$ few units). We choose the parameters corresponding to a typical active region such that $L = 50\,\mathrm{Mm}$, $d = 50\,\mathrm{Mm}$ and $q = 10^2\ \mathrm{T}\cdot\mathrm{Mm}^2$ (e.g. see Manoharan et al.1996), which yields a maximum photospheric field $= 0.04\,\mathrm{T}$ ($= 400\,\mathrm{G}$). If one puts also the current $I_0 = -7\,\mathrm{TA}$, then for the unstable value of major radius $R \equiv R_m$ the radius of the tube has the value $a \equiv a_m \approx 31\,\mathrm{Mm}$.

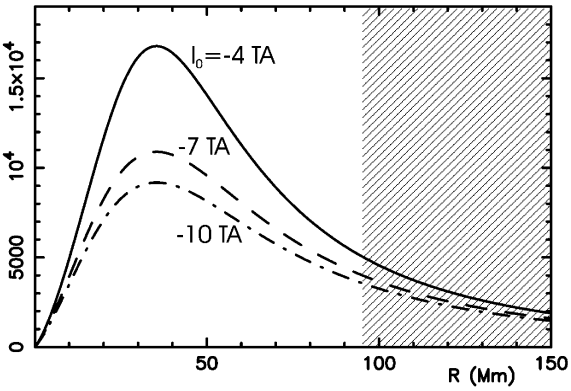

Fig. 3. The total toroidal current I in the ring versus the radius R of the flux tube at three different values of I_0. The region of the unstable equilibrium, as estimated in the Appendix, is shaded.

2.2. Approximate analytical expressions for the magnetic field

We use the tubal system of coordinates (ρ, ϕ, θ), ρ is the distance from the axis of the tube and ϕ is the angle between radius ρ and the plane of symmetry $x = 0$, while θ measures the angular arc length of the tube from the positive direction of y-axis. Since the flux tube in our model is assumed to be thin in comparison with its radius of curvature R and the characteristic size L, the corresponding force-free condition in zero order approximation by small parameters a/R and a/L is the same as for the straight tube. So in the above tubal coordinates the force-free condition can be written at $0 < \rho \le a$ as follows

$$\frac{\rho}{2}\frac{\partial}{\partial \rho}(B^2_{\phi_{\rm in}} + B^2_{\theta_{\rm in}}) + B^2_{\phi_{\rm in}} \approx 0, \tag{11}$$

where the azimuthal magnetic field component

$$B_{\phi_{\rm in}} \approx \frac{\mu_0 I \rho}{2\pi a^2} \tag{12}$$

corresponds to the uniformly distributed toroidal current I. Eqs. (11)–(12) give the toroidal field inside the tube

$$B_{\theta_{\rm in}} \approx \mathrm{sign}(I_0) \left[B^2_{\theta_{\rm R}} + \frac{\mu_0^2 I^2}{2\pi a^4}(a^2 - \rho^2) \right]^{1/2}, \tag{13}$$

where the toroidal field on the surface of the tube

$$B_{\theta_{\rm R}} \approx \frac{\mu_0 I_0}{2\pi R} \tag{14}$$

is followed from the appropriate approximation of the external toroidal field

$$B_{\theta_{\rm ex}} = \frac{\mu_0 I_0}{2\pi}[y^2 + (z+d)^2]^{-1/2}, \tag{15}$$

which is produced by the sub-photospheric line current I_0.

Both internal and external toroidal fields can be sewed by using the following formula:

$$\boldsymbol{B}_\theta = \frac{\mu_0 I_0}{2\pi}\left\{\left[\frac{1}{R^2}+\frac{2\chi(a-\rho)}{a^2}\frac{I^2}{I_0^2}\left(1-\frac{\rho^2}{a^2}\right)\right]^{1/2}+ [y^2+(z+d)^2]^{-1/2}-R^{-1}\right\}\hat{\boldsymbol{\theta}}. \quad (16)$$

where

$$\hat{\boldsymbol{\theta}} = \left(0, -\frac{z+d}{r_\perp}, \frac{y}{r_\perp}\right), \quad (17)$$

$$\rho = \left[x^2+(r_\perp-R)^2\right]^{1/2}, \quad (18)$$

$$r_\perp = [y^2+(z+d)^2]^{1/2} \quad (19)$$

and $\chi(X)$ stands for the Heaviside function such that $\chi = 1$ if $X > 0$ and $\chi = 0$ otherwise. Eq. (16) describes the toroidal magnetic field inside the flux tube only in zero order approximation by small parameters a/R and a/L, which is sufficient for determination of the topology in our configuration (see Sect. 3 for more details).

We also determined with the same accuracy, the poloidal magnetic field everywhere in the coronal volume. Inside the flux tube Eq. (12) yields it with the desired accuracy, outside the tube it is approximately a superposition of the point sources field

$$\boldsymbol{B}_q = q\left(\frac{\boldsymbol{r}_+}{|\boldsymbol{r}_+|^3}-\frac{\boldsymbol{r}_-}{|\boldsymbol{r}_-|^3}\right), \quad (20)$$

$$\boldsymbol{r}_\pm = (x\mp L,\, y,\, z+d), \quad (21)$$

and of the field $\boldsymbol{B}_{I_{\rm ex}}$ produced by the line current I in the ring of radius R. In order to derive $\boldsymbol{B}_{I_{\rm ex}}$ and the proper sewing function $\boldsymbol{B}_I$, it is helpful to represent the magnetic field in terms of the vector potential, which due to the symmetry of our configuration about x-axis can be reduced to only one non-vanishing θ-component $A_I(r_\perp, x)$, so that

$$\boldsymbol{B}_I = \nabla\times(A_I\,\hat{\boldsymbol{\theta}}) = -\frac{\partial A_I}{\partial x}\frac{\boldsymbol{r}_\perp}{r_\perp}+\left(\frac{\partial A_I}{\partial r_\perp}+\frac{A_I}{r_\perp}\right)\hat{\boldsymbol{x}}. \quad (22)$$

From here and Eq. (12) one can derive A_I inside the tube

$$A_{I_{\rm in}} \approx \frac{\mu_0 I}{2\pi}\left(\text{const}-\frac{\rho^2}{2a^2}\right). \quad (23)$$

Outside the flux tube, A_I is well approximated by the potential of the ring determined by

$$A_{I_{\rm ex}} \approx \frac{\mu_0 I}{4\pi}\oint\frac{\hat{\boldsymbol{\theta}}\cdot{\rm d}\boldsymbol{r}'}{|\boldsymbol{r}-\boldsymbol{r}'|} \equiv \frac{\mu_0 I R}{4\pi(R^2+r_\perp^2+x^2)^{1/2}}\int_0^{2\pi}\frac{\cos\theta'\,{\rm d}\theta'}{(1-\upsilon\,\cos\theta')^{1/2}},$$

where

$$\upsilon = \frac{2r_\perp R}{R^2+r_\perp^2+x^2}. \quad (24)$$

The above integral is expressed in terms of the complete elliptic integrals of the first and second kinds, $K(k)$ and $E(k)$, as follows:

$$A_{I_{\rm ex}}(x, r_\perp) \approx \frac{\mu_0 I}{2\pi}\sqrt{\frac{R}{r_\perp}}\,\mathcal{A}(k), \quad (25)$$

in which

$$\mathcal{A}(k) \equiv k^{-1}\left[(2-k^2)\,K(k)-2\,E(k)\right] \quad (26)$$

and

$$k \equiv 2\sqrt{\frac{r_\perp R}{(r_\perp+R)^2+x^2}}. \quad (27)$$

There is a small mismatch at $\rho = a$ between $A_{I_{\rm ex}}$ and $A_{I_{\rm in}}$, which can be eliminated by using, instead of $A_{I_{\rm in}}$, the following expression:

$$\tilde{A}_{I_{\rm in}} \approx \frac{\mu_0 I}{2\pi}\sqrt{\frac{R}{r_\perp}}\,\left[\mathcal{A}(k_{\rm a})+\mathcal{A}'(k_{\rm a})(k-k_{\rm a})\right], \quad (28)$$

where

$$\mathcal{A}'(k) \equiv \frac{\rm d}{{\rm d}k}\mathcal{A}(k) = \frac{\left(2-k^2\right)E(k)-2\left(1-k^2\right)K(k)}{k^2\left(1-k^2\right)} \quad (29)$$

and

$$k_{\rm a} = 2\sqrt{\frac{r_\perp R}{4r_\perp R+a^2}} \quad (30)$$

is the value such that $k = k_{\rm a}$ at $\rho = a$ and always $k_{\rm a} < 1$, so $\mathcal{A}(k_{\rm a})$ and $\mathcal{A}'(k_{\rm a})$ are regular functions of $r_\perp$. One can show that in zero order approximation by a/R Eq. (28) reduces to Eq. (23), while $\tilde{A}_{I_{\rm in}}$ and $A_{I_{\rm ex}}$ at $\rho = a$ are equal to each other together with their first derivatives, so the corresponding sewing function is

$$A_I = \chi(a-\rho)\,\tilde{A}_{I_{\rm in}}+\chi(\rho-a)\,A_{I_{\rm ex}}. \quad (31)$$

By using this and Eq. (22) one can easily derive now an explicit formula for $\boldsymbol{B}_I$ and so for the whole magnetic field. We do not present this $\boldsymbol{B}_I$ here because of the length of this formula, but the above consideration shows how the whole magnetic field in our configuration can be analytically described in terms of continuous expressions with an accuracy which is sufficient for investigating the magnetic topology.

3. Appearance, bifurcation and disappearance of BPs

3.1. Definition and role of BPs

The BP is a segment of the photospheric inversion line (IL), around which the field lines have a dip, so that there are coronal field lines touching this segment and returning to corona. The corresponding criterion for the BP existence is given by:

$$\boldsymbol{B}_{\rm h}\cdot\boldsymbol{\nabla}_{\rm h}B_z|_{\rm IL} > 0, \quad (32)$$

where h and IL, respectively, stand for the horizontal components of vectors and the inversion line of the normal field B_z (see Seehafer 1986 and in more detail Titov et al.1993).

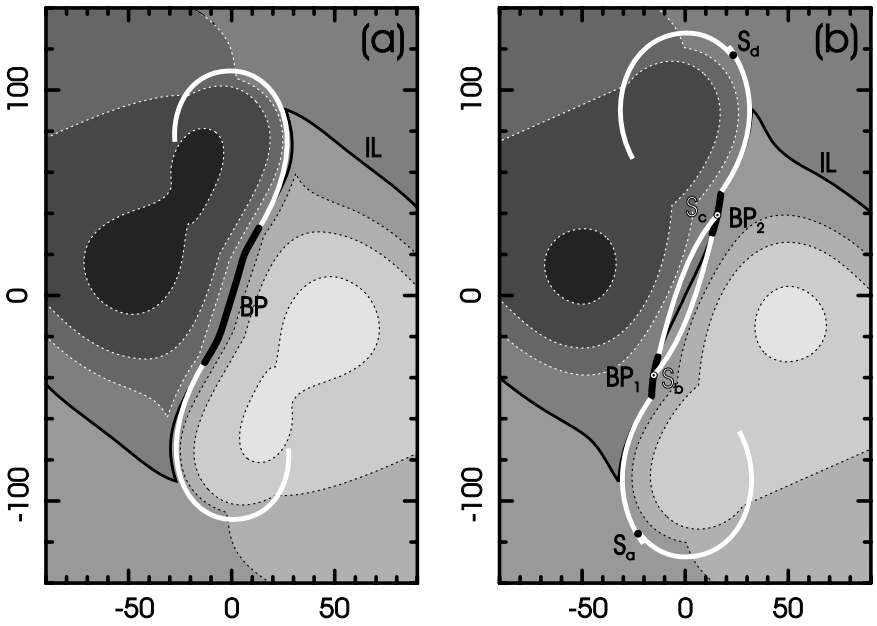

Fig. 4a and b. Effective magnetograms of the configuration (at the following parameters defined in Sect. 3: $L = 50$ Mm, $d = 50$ Mm, $q = 100\ \mathrm{T}\cdot\mathrm{Mm}^{-2}$, $N_t = 5$, $I_0 = -7$ TA) before (**a**), $R = 85$ Mm, and after (**b**), $R = 98$ Mm, bifurcation of the bald patch – the thickest black line; the inversion line and photospheric traces of the corresponding separatrix surfaces are represented, respectively, by black and white solid lines, while contours of $B_z = \pm 100,\ \pm 200,\ \pm 400$G (dashed thin lines) are filled depending on the strength of the field with lighter or darker grey colors, correspondingly, in positive and negative polarities.

This criterion requires that the horizontal field at BPs must be directed from negative to positive polarity, i.e. in the opposite way as compared to the normal parts of IL. It means that in the generic case a BP, if present, has a finite length. Therefore the magnetic field topology caused by the presence of BPs is structurally stable, i.e. a small perturbation of magnetic field in the configuration containing BPs may only slightly change the direction of this horizontal field and so the length and position of BPs. Thus, the topological structure caused by BPs is robust, in particular, with respect to breaking out of possible symmetry in configuration or to a small inaccuracy of the approximation used for calculating the magnetic field. These two circumstances are quite important for further analysis of our model.

The BPs are interesting in the following respects: first of all, they define separatrices where the current sheets can develop. Secondly, the separatrices starting at two distinct BPs may intersect along a topologically special field line, called separator, where the magnetic reconnection is quite plausible (see Sect. 4 and Bungey et al.1996). It is very important here that, contrary to the traditional definition, such a separator is not a field line connecting two null points (whose appearance in corona is usually quite problematic). Thirdly, during evolutions of magnetic configurations the BPs may be precursors of the null point emergence into the coronal field (Bungey et al.1996), thereby giving another association with the magnetic topology and reconnection process in corona. Finally, the BPs are thought to be the locations where chromospheric material can be lifted up and so they are linked with the physical processes in prominences (Titov et al.1993) and, in particular, in their feet (Aulanier and Démoulin 1998a).

3.2. Presence of BPs in the model

A BP in our model is first formed at the center of the configuration when the flux tube begins to emerge above the photosphere (Fig. 4a). As the tube emerges further (R increases), the BP bifurcates (Fig. 4b), then the distance between its parts increases, they shrink and finally disappear. Such an evolution of the magnetic topology is proposed here as a typical one for emerging twisted flux tubes. Our simplified model enables us below to estimate the critical radii for the appearance (R_a), bifurcation (R_b), and disappearance (R_d) of the BP.

Since our flux tube is in a force-free equilibrium, the subphotospheric sources produce the transverse field $\boldsymbol{B}_q$ of nearly the same value as the corresponding component created by the whole ring current of the tube. So the magnetic field inside the tube and in its vicinity is mainly a superposition of the azimuthal $\boldsymbol{B}_\phi$ and toroidal $\boldsymbol{B}_\theta$ components. This makes it possible to estimate the conditions of appearance and bifurcation of BPs in this situation.

Indeed, the field lines of $\boldsymbol{B}_\phi$ at a distance ρ from the tube axis have a curvature ρ^{-1}, while the field lines of $\boldsymbol{B}_\theta$ at the same distance from the axis but in the lower part of the apex have a curvature $(R-\rho)^{-1}$. Thus at this point the field lines of the whole field $\boldsymbol{B}_\phi + \boldsymbol{B}_\theta$ touch a saddle surface whose main curvatures are ρ^{-1} and $-(R-\rho)^{-1}$ (see Fig. 5), which implies a contact of second order at the corresponding point. To estimate the field line curvature at this point, it is necessary to place the system of coordinates (ξ, η, ζ) (Fig. 5a), such that the saddle surface satisfies

$$\zeta = \frac{\xi^2}{2\rho} - \frac{\eta^2}{2(R-\rho)}\,. \tag{33}$$

Its intersection with the vertical plane, given by

$$\xi = s\sin\vartheta, \tag{34}$$

$$\eta = s\cos\vartheta, \tag{35}$$

determines approximately the field line passing through the indicated point of contact. Here the parameter s is a distance from this point along a straight line tangent to such a field line and

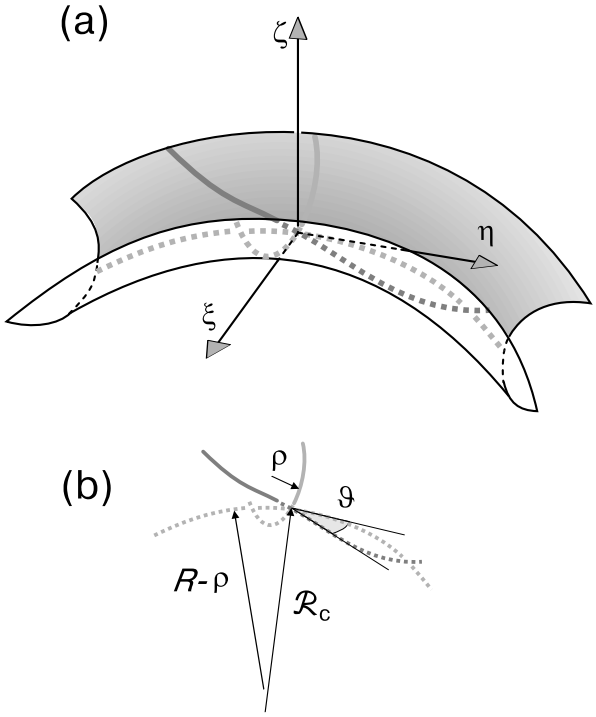

Fig. 5a and b. Shape of magnetic field lines below a thin twisted flux tube. **a** Field lines are located on a saddle surface which has a point of contact of the second order with the photospheric plane $\zeta = 0$ (when the apex of the tube emerges into corona). **b** The main radii of curvature ρ and $R - \rho$ of such a saddle surface and the radius of curvature $\mathcal{R}_c$ of the field line.

directed at pitch angle ϑ with respect to the axis of the tube. It follows from (33)–(35) then, that locally the field line under consideration is parametrically represented by

$$\zeta \approx \frac{s^2}{2}\left(\frac{\sin^2\vartheta}{\rho} - \frac{\cos^2\vartheta}{R-\rho}\right) \tag{36}$$

and (34)–(35). Differentiating this expression twice to s gives an approximate value of curvature of the field line, namely

$$\mathcal{R}_c^{-1} \approx \frac{\sin^2\vartheta}{\rho} - \frac{\cos^2\vartheta}{R-\rho} = (B_\phi^2 + B_\theta^2)^{-1}\left(\frac{B_\phi^2}{\rho} - \frac{B_\theta^2}{R-\rho}\right). \tag{37}$$

So for $\mathcal{R}_c^{-1} > 0$ or

$$B_\phi^2/B_\theta^2 > \rho/(R-\rho), \tag{38}$$

a BP will be present at the center of our configuration. $B_\phi(a)$ is related to the number of winding N_t in torus as follows

$$B_\phi(a)/B_\theta \approx N_t a/R. \tag{39}$$

By rewriting $B_\phi(\rho) = B_\phi(a)\, b(\rho)$ (with $b(\rho) = \rho/a$ for $\rho \le a$ and $b(\rho) = a/\rho$ for $\rho \ge a$) one can obtain from Eq. (38)

$$f(\rho) \equiv \left(\frac{N_t a}{R}\right)^2 b^2(\rho) - \frac{\rho}{R-\rho} > 0. \tag{40}$$

For a given magnetic configuration, $f(\rho)$ is maximal at $\rho = a$ if N_t is large enough. This means that as N_t increases, a BP appears first at the border of the current region and then it extends outside this region. So with the emergence of the flux tube, a BP will first appear in the current region ($\rho \le a$) and then it will disappear in the potential region ($\rho > a$). Thus the limiting case when the BP is present only at $\rho = a$ gives the condition of its existence.

3.3. Appearance of BP

Consider what Eq. (40) yields first for the interior of the flux tube ($\rho < a$) where there is a uniform distribution of the toroidal current density. In such a tube

$$B_\phi(\rho) \approx B_\phi(a)\,\rho/a, \tag{41}$$

Substituting (41)–(39) into (40) and using

$$R = \rho + d, \tag{42}$$

we obtain after some transformations

$$(\rho/d)^2 - (N_t^2 - 2)(\rho/d) + 1 \lesssim 0. \tag{43}$$

This inequality has a solution if

$$N_t \gtrsim 2, \tag{44}$$

which means that BP does not appear at the center of configuration if the flux tube is not twisted enough or, in other words, if the total current in the tube is not sufficiently large. The solution of (43) is $(\rho_a/d) \lesssim (\rho/d) \lesssim (d/\rho_a)$, where

$$\rho_a/d = 4/\left(N_t + \sqrt{N_t^2 - 4}\right)^2 \tag{45}$$

determines the minimal values of ρ_a and $R_a = d + \rho_a$ at which the BP appears in the configuration. The upper bound (d/ρ_a) of (ρ/d) has no a real meaning, since it corresponds to $\rho > a$, while we use above the expression of B_ϕ valid only for $\rho \le a$. It is also necessary in this case that $\rho_a \le a$, so that a BP would exist at least at $\rho = a$, which yields

$$4/\left(N_t + \sqrt{N_t^2 - 4}\right)^2 \lesssim a/d. \tag{46}$$

Thus, for the presence of a BP formed by some of the interior field lines, both conditions (44) and (46) must be fulfilled. The BP appears at the photospheric level when the flux tube radius reaches $R_a = d + \rho_a$, where ρ_a is given by Eq. (45)

3.4. Bifurcation of BP

Let us do a similar analysis for the exterior of the flux tube to identify precisely when a BP is present. By assuming $\rho \ll R$ again or $(\rho/d) \ll 1$ and using (39) we obtain

$$B_\phi(\rho) \approx B_\phi(a)\, a/\rho \approx N_t\, a^2\, B_\theta/(R\rho), \tag{47}$$

so that (38) yields now $(\rho/d) \lesssim (\rho_b/d)$, where

$$\rho_b/d = (N_t\, a^2/d^2)^{2/3} \tag{48}$$

determines values $\rho_{\rm b}$ and $R_{\rm b} = d + \rho_{\rm b}$, starting from which the BP exists only in a bifurcated form. This estimation implies that $a/d << (\rho_{\rm b}/d) < 1$, which is equivalent to

$$1/N_t^2 \lesssim a/d << 1/\sqrt{N_t}. \quad (49)$$

In fact numeric computations yield $\rho_{\rm b}$ comparable in value with R ($\rho_{\rm b}/R \approx 0.4$ in Fig. 4), so Eq. (48) is less accurate than Eq. (45).

3.5. Disappearance of BPs

After bifurcation of the BP its parts diverge with growing R from each other and shrink near the legs of the flux tube. They completely disappear when these legs become so inclined that the internal twist of the tube can no longer produce a local dip. By approximating any field line near the legs as a straight helix with the corresponding pitch angle one can see that the helix ceases to touch the photosphere when the inclination of the tube axis toward the horizontal exceeds the pitch angle. So for a given field line with some B_ϕ/B_θ the critical tangent of the tube inclination is

$$\frac{\sqrt{R^2-d^2}}{d} \approx \frac{B_\phi}{B_\theta}\,, \quad (50)$$

which has a maximum at $\rho \approx a$. Therefore the BPs disappear at $R = R_{\rm d}$ such that

$$\frac{\sqrt{R_{\rm d}^2-d^2}}{d} \approx \frac{aN_t}{R_{\rm d}}\,, \quad (51)$$

from where we obtain finally

$$R_{\rm d} \approx d\sqrt{\frac{1+\sqrt{1+(2aN_t/d)^2}}{2}} \approx \sqrt{adN_t}\,. \quad (52)$$

3.6. Summary of the existence of BPs

In summary, one can say that under the assumptions used, the more twisted the flux tube (i.e., the larger N_t), the earlier BP appears (Eq. 45) and the longer it lasts. The appearance of a BP does not depend on minor radius a of the tube (Eq. [45]), while the critical radii $R_{\rm b}$ and $R_{\rm d}$ for the BP bifurcation and disappearance decrease with a (see Eq. [48] and Eq. [52]). In solar active regions, however, the parameter aN_t is usually of the order of d, so that the BPs must exist in twisted configurations in a wide range of parameters. For example, for the mentioned above typical parameters the BP appears at $R_{\rm a} \approx 70$ Mm, bifurcates at $R_{\rm b} \approx 91$ Mm and disappears at $R_{\rm d} \approx 106$ Mm. Thus the bald patches are present in the range $R_{\rm d} - R_{\rm a}$ comparable with the active region size L, which must correspond to an essential period in the emerging of the twisted flux tube.

4. Global topological structure caused by bald patches

The topology of coronal magnetic field is completely described by the whole set of separatrix surfaces, which will be called the topological skeleton of configuration. In our model this skeleton is very simple when $R_{\rm a} \le R \le R_{\rm b}$, since it is determined by a single separatrix surface associated with one BP. With further expanding of the flux tube this BP bifurcates at $R = R_{\rm b}$, so that each new BP gives rise to a distinct separatrix. Such a bifurcated structure exists for all R from the interval $R_{\rm b} < R \le R_{\rm d}$. In smaller interval $R_{\rm b} < R \le R_{\rm ds}$ it has an especially interesting complexity and deserves a detailed consideration. It is helpful to represent the skeleton in a dual form (see diagram in Fig. 6): first as a union of two distinct separatrices formed by the field lines starting from different bald patches BP_1 and BP_2 and second as a union of upper and lower one-connected surfaces originating from the corresponding photospheric traces of the field lines.

Due to the symmetry of our configuration the form and the structure of separatrices associated with BP_1 and BP_2 are obtained from each other by simple reverse of the field line arrows and rotation around z-axis on the angle π, so it is sufficient to consider only one of these separatrices. The segment $\mathrm{A_1B_1}$ of the IL represents in Fig. 6 (top right) the bald patch BP_1 divided by the point $\mathrm{S_b}$ into the "inner" $\mathrm{S_bB_1}$ and "peripheral" $\mathrm{A_1S_b}$ parts. All the field lines touching BP_1 start from the one photospheric trace C_5 of the separatrix under consideration. However, the field lines touching the inner and peripheral parts of BP_1 end up, respectively, at the traces C_3 and C_1. Such a structure is possible due to the presence of the special field line, which starts from the point $\mathrm{S_a}$ (a middle point of C_5) and ends up at the point $\mathrm{S_d}$ (an edge point of C_1). In the skeleton, this is the only field line touching the IL twice – at the points $\mathrm{S_b}$ and $\mathrm{S_c}$ belonging, respectively, to BP_1 and BP_2.

The latter, in particular, explains why such a line is common for both separatrices caused by BP_1 and BP_2. Its central arc $\mathrm{S_bS_c}$ determines the curve, along which these separatrices intersect. The peripheral arc $\mathrm{S_aS_b}$ or $\mathrm{S_cS_d}$ serves as a line of contact of the separatrices, since it is always a part of the border for one of them. Thus, there are X- and T-type intersections of the separatrices, respectively, along the central and peripheral parts of this special field line, which is called "separator" or "BP-BP line". We would like to emphasize that this is not a traditional separator defined as a "null-null line" connecting two null points of magnetic field (see the definition, e.g., in Lau & Finn 1990). In our configuration such null points never appear due to the non-vanishing toroidal component produced by the sub-photospheric current $I_0 (\neq 0)$.

Alternatively, the topological skeleton can be represented as a union of two one-connected surfaces, where the upper and lower ones are "woven" from the field lines anchored, respectively, at the traces C_1, C_2 and C_3, C_4 (see the low half of the diagram in Fig. 6). These surfaces contact each other along the separator in the above described manner. The lower surface has a wedge-like apex and stretches along the IL by isolating a compact arcade of field lines, which can be naturally identified with a new emerging magnetic flux. The upper surface represents a wrapped and relatively wide ribbon with a corner bending along the separator – it stretches far into corona and it ends at the photosphere in the C_1 and C_2. A 3D view on the resulting topological skeleton of the configuration is shown in Fig. 7.

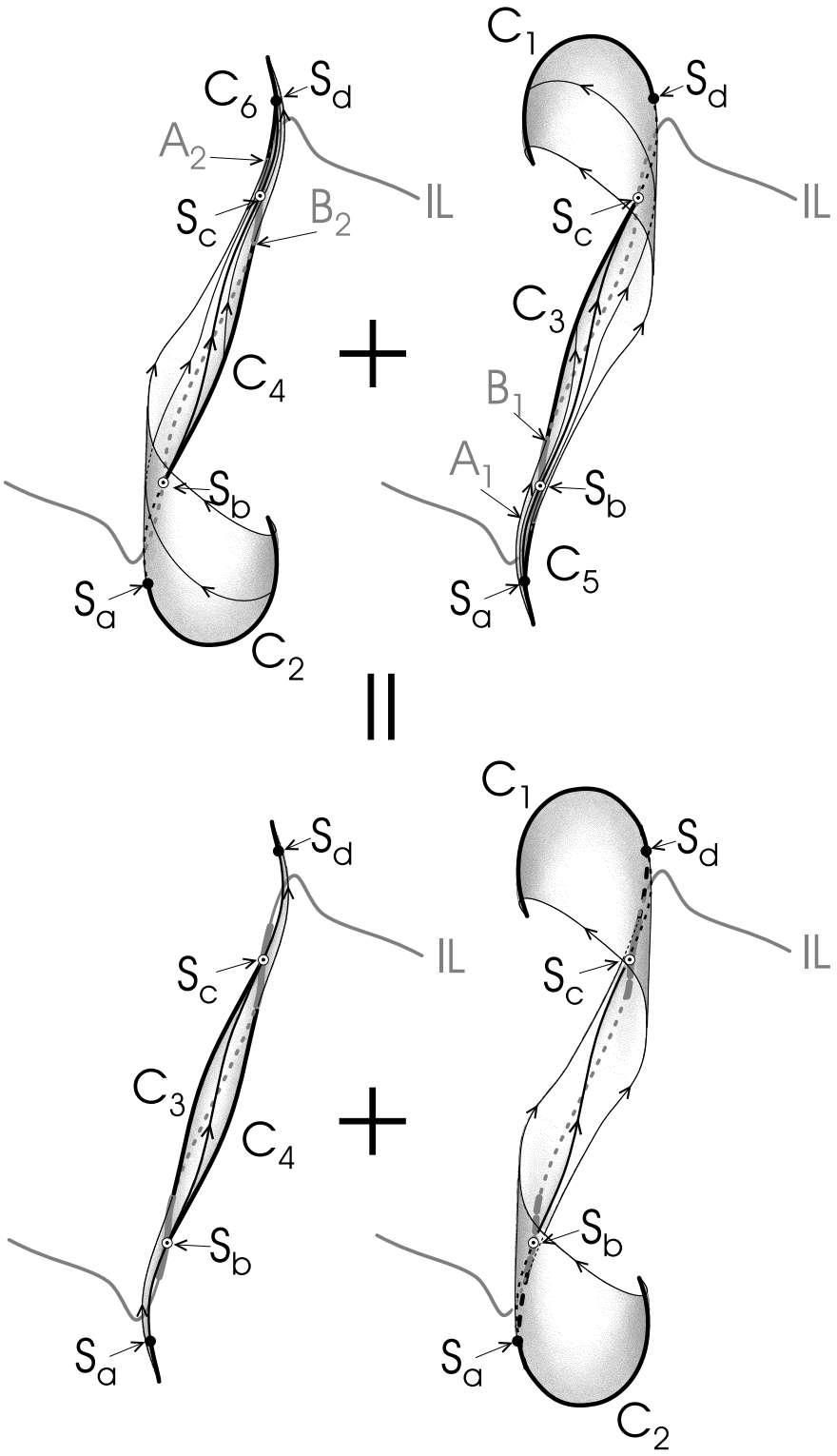

Fig. 6. The topological skeleton of the twisted configuration with the separator anchoring the photosphere at the points S_a and S_d and touching it at the points S_b and S_c of the inversion line (IL): it is either a union of two separatrices formed by the field lines which touch the bald patches A_1B_1 and A_2B_2 (top) or a union of the lower and upper surfaces formed by the field lines which are anchored, respectively, at the photospheric traces C_3, C_4 and C_1, C_2 (bottom).

With growing R, the peripheral parts of BPs together with the associated parts of separatrices shrink more rapidly than their inner parts. Therefore, at $R = R_{\rm ds} < R_{\rm d}$ the peripheral parts completely disappear and for R such that $R_{\rm ds} < R \le R_{\rm d}$ this intersection or separator ceases to exist; the BPs continue to shrink in size as R increases and completely disappears at $R = R_{\rm d}$. For larger values of R there are no BPs or null points of magnetic field and so the mapping along field lines from one photospheric polarity to the other is continuous. Thus the magnetic configuration becomes topologically equivalent to a simple arcade.

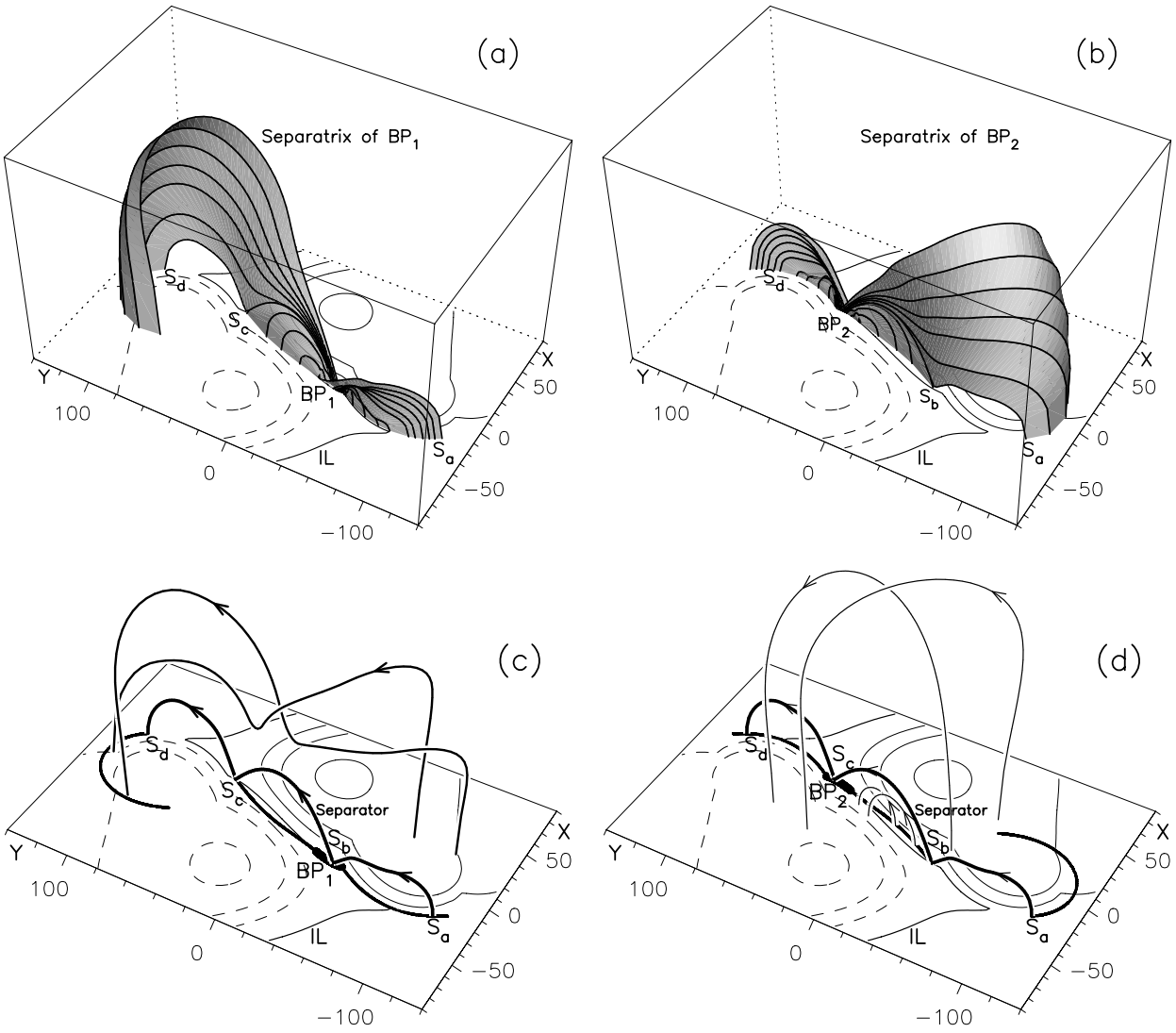

Fig. 7a–d. A 3D view on the topological skeleton of the twisted configuration (for esthetics the vertical height (z) has been changed by the function $30\sqrt{z}$). The separatrix associated with BP_1 (resp. BP_2) is drawn in **a** (resp. **b**) and its intersection with the photosphere is shown in **c** (resp. **d**). The separatrices intersection (separator) in shown in **c** and **d** by a thick line. Examples of field lines outside separatrices are given by pairs: in **c** a pair belonging to the flux tube, and in **d** one pair above and one below the flux tube. The parameters of the model and iso-contours of the vertical field B_z are the same as in Fig. 4.

5. Topological equivalence of the twisted and untwisted configurations

It is worth comparing the topology of twisted and untwisted configurations having similar distributions of the normal magnetic field at the photosphere. Such an untwisted configuration can be modeled by two bipolar groups of charges placed below the photosphere on some depth. Its topological evolution was investigated by Titov et al.(1993) and Bungey et al.(1996), who showed that with growing the internal bipole it passes through the stages similar to ones for our twisted configuration: first, the appearance and development of one BP, second, its bifurcation and appearance of separator, and third, the disappearance of the separator and then the BPs themselves due to their shrinkage. The stage characterized by the presence of the separator is illustrated in Fig. 8 (to be compared with Fig. 6), from where it follows that the topological skeletons of this potential and our twisted configurations are equivalent, i.e. one can obtain them from another by suitable continuous deformations.

On the other hand, they have rather different geometrical forms, notably, the shapes of the upper separatrix surface formed by the field lines which are anchored at the traces C_1 and C_2. When moving from the separator along this surface it is concave and strongly wrapped for the twisted configuration, and convex and not so much curved for the potential configuration. In the result the traces C_1 and C_2 are very curved and relatively distant from the IL in the first case, and less curved and located nearby the IL in the second case. Because of the difference in convexity of the separatrices the traces C_1, C_2 and C_5, C_6 are counter- and co-directed relative to adjacent parts of the IL in the first

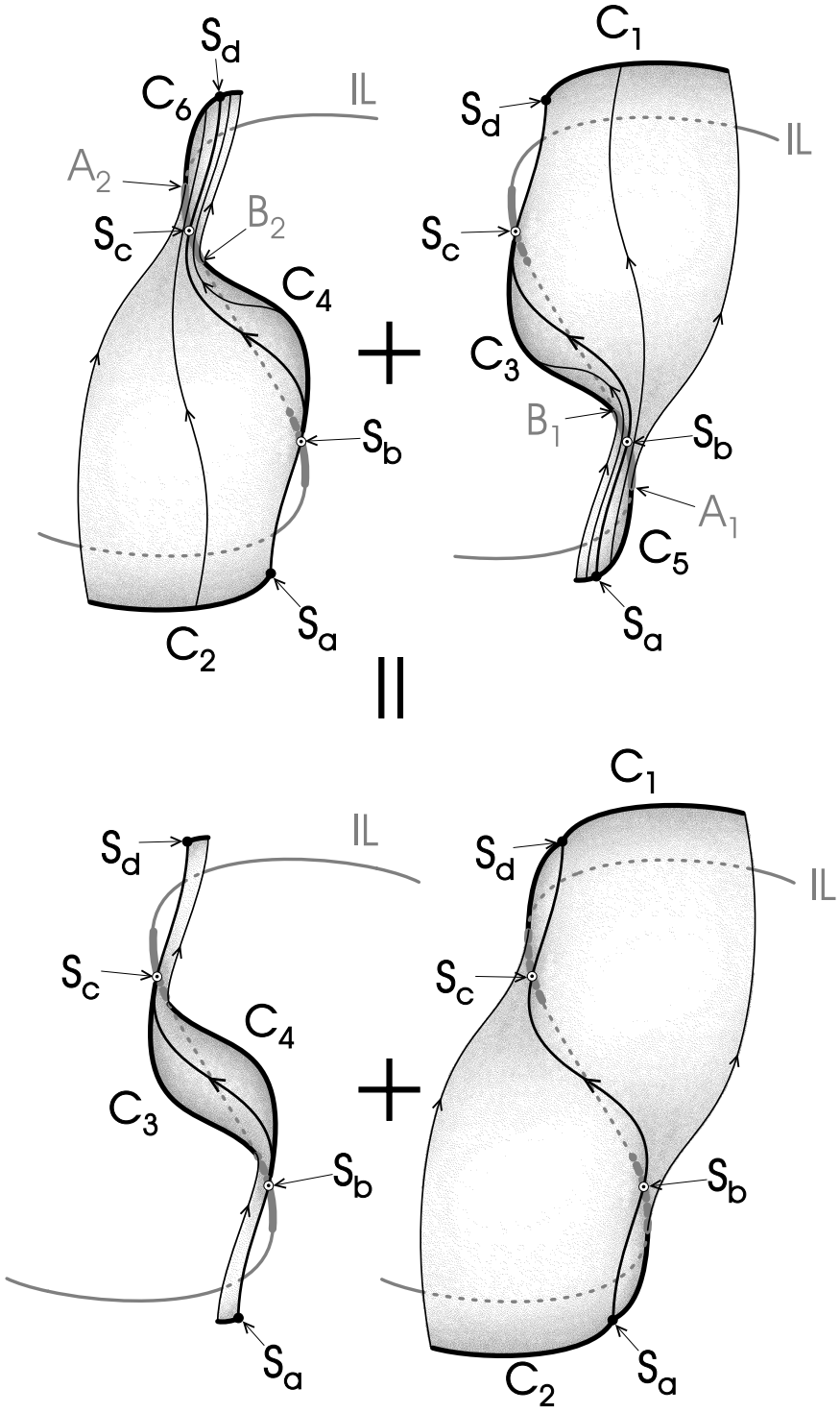

Fig. 8. The topological skeleton of the potential configuration with the separator anchoring the photosphere at the points S_a and S_d and touching it at the points S_b and S_c of the inversion line (IL): it is either a union of two separatrices formed by the field lines which touch the bald patches A_1B_1 and A_2B_2 (top) or a union of the lower and upper surfaces formed by the field lines which are anchored, respectively, at the photospheric traces C_3, C_4 and C_1, C_2 (bottom).

and second cases, respectively. The traces C_3 and C_4 are quite similar in this sense for both types of configurations.

As was discussed earlier, the generation of strong currents and flare energy release probably occurs at the separator and separatrices, so the flare ribbons and X-ray brightenings must be located along the photospheric traces of separatrices. Therefore, the above mentioned features in location and form of the traces C_1 and C_2 can be helpful for distinguishing two types of flares occurring in globally twisted or untwisted magnetic fields.

6. Relative location of topological features and currents

In previous studies (e.g. Titov et al.1993, Bungey et al.1996) separatrix surfaces are mainly determined by locations and intensities of the photospheric field concentrations. So the separatrices were present even in potential configurations and modified

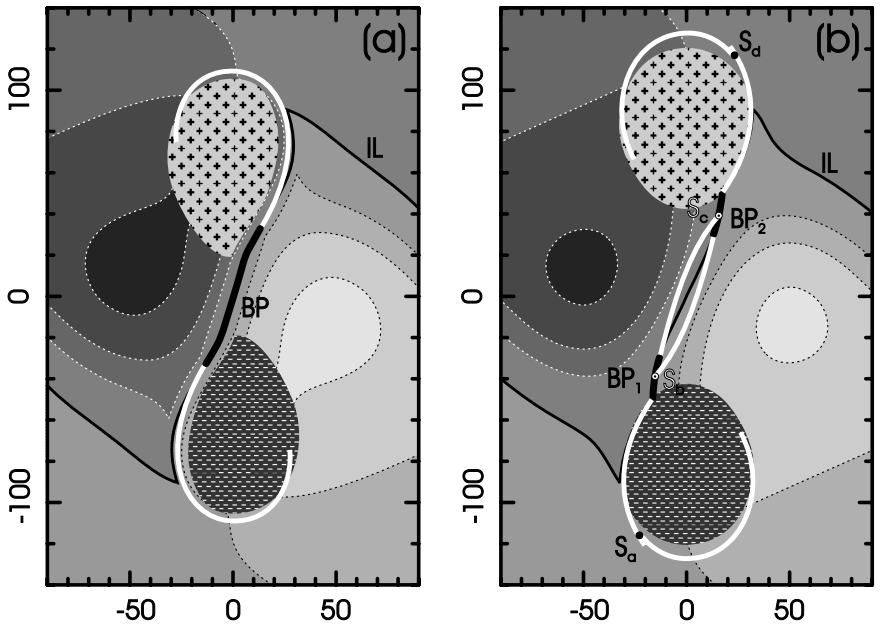

Fig. 9a and b. Relative location on the photosphere of the concentrations of vertical current density j_z with respect to BPs and associated traces of separatrices. The regions of positive and negative concentrations are dashed by black $+$ and white $-$ on the light and dark grey backgrounds, respectively. They are superimposed on the corresponding effective magnetograms shown in Fig. 4.

to a topologically equivalent form by the corresponding incorporation of electric currents. It is not the case, however, for the above considered twisted configuration – in the limit of vanishing toroidal current I, the topological features disappear and the configuration becomes topologically trivial. This may serve as an indication of a possibly closer relationship between the current distribution and magnetic topology in active regions.

To verify this point, let us determine the current density distribution in our configuration as

$$\boldsymbol{j} \approx \chi(a-\rho)\left(\frac{I}{\pi a^2}\hat{\boldsymbol{\theta}} - \frac{1}{\mu_0}\frac{\partial B_{\theta_{\rm in}}}{\partial \rho}\hat{\boldsymbol{\phi}}\right), \tag{53}$$

where $\hat{\boldsymbol{\phi}} = \hat{\boldsymbol{\rho}} \times \hat{\boldsymbol{\theta}} = \hat{\boldsymbol{\rho}} \times (\hat{\boldsymbol{r}}_\perp \times \hat{\boldsymbol{x}}) = (\hat{\boldsymbol{\rho}} \cdot \hat{\boldsymbol{x}})\hat{\boldsymbol{r}}_\perp - (\hat{\boldsymbol{\rho}} \cdot \hat{\boldsymbol{r}}_\perp)\hat{\boldsymbol{x}}$ and so in Cartesian coordinates

$$\hat{\boldsymbol{\phi}} = \left(\frac{R-r_\perp}{\rho}, \frac{xy}{\rho r_\perp}, \frac{x(z+d)}{\rho r_\perp}\right).$$

These formulas together with Eqs. (13)–(14) and Eqs. (17)–(19) define the current density distribution everywhere in the flux tube and, in particular, on the photosphere if one puts $z = 0$ in these expressions.

Fig. 9 depicts the location of the vertical currents (j_z) together with the separatrix traces. When the apex of the flux tube only just appears above the photosphere, the BP and associated separatrix are located well inside the current region. With further emerging of the flux tube the separatrix moves closer to the border of the current region (Fig. 9a) and then bifurcates by producing the separator at the border of the current region (Fig. 9b). Just before disappearance of the BPs they are still located close to the current region, because the azimuthal field component B_ϕ, responsible for their presence, has a maximum value there (see Eq. [51]).

As mentioned earlier, the separatrices are likely places for the formation of strong current layers and so for the development of magnetic reconnection. This process converts the free magnetic energy into the energy of different kinds, in particular, into the fluxes of heat and accelerated particles, which are channeled along the field lines towards the photosphere. Therefore, the corresponding manifestations must be observed at the photospheric traces of separatrices and, according to the above consideration, near borders of the current density concentrations. Indeed, the observations show that Hα kernels and electron precipitation appear preferentially at the border of observed current concentrations (see Li et al.1997 and references therein). Thus, the systematic location of the separatrix traces at the border of the current concentrations give a natural explanation of this well-established observational fact.

7. Discussion and conclusions

Magnetic topology is a key ingredient for understanding where in the solar corona the magnetic energy release occurs. It is determined in terms of the coronal field-line connectivity, which is obtained by integrating the equations of field lines. The magnetic field itself can be in turn computed by integrating force-free equations from the photospheric distributions of the vertical magnetic field and current density (which are deduced, for instance, from observations). So one can expect that the topology of magnetic field structures weakly depends on small details of such distributions. This makes it useful to study the nontrivial topology of elementary magnetic cells, which are simple characteristic constituents of more complicated fields in real active regions. Titov et al.(1993), Bungey et al.(1996) and Démoulin et al.(1996a) have done it for quadrupolar configurations with potential and linear force-free fields. The aim of this paper is to extend such an analysis to magnetic configurations having concentrated currents, which are routinely observed. Such a force-free configuration is modeled here by a twisted flux tube, whose loop-like body is embedded into a potential bipolar field.

A similar, but not force-free configuration, has been considered previously by Démoulin et al.(1996b).

We investigate first the presence of the segments at the photospheric inversion line where the coronal field lines touch the photosphere (called BPs). The field lines starting at a BP form a separatrix surface, where the field-line connectivity suffers a jump. As the flux tube emerges, a BP appears first near the apex of the tube, then by growing in size it bifurcates just under this apex and with subsequent shrinking of the bifurcated parts the BP disappears as soon as the flux tube protrudes well enough into corona. The bifurcation of the BP leads to an appearance of a generalized separator field line in the result of intersection of two separatrix surfaces starting at the different bifurcated parts of BP. This kind of separator is similar to the one found by Bungey et al.(1996) for potential and linear force-free fields and it can be considered as an appropriate generalization of the traditional separator which connects two null points of magnetic field (see Titov 1999). In comparison with these cases, the presence of the concentrated current in our twisted configuration significantly facilitates an appearance of such a separator. It is shown here that this separator may exist in this configuration when the radius of curvature of the flux tube varies within the size of the active region. Although the considered configuration has an axis of symmetry, the obtained results must also be valid for similar non-symmetric configurations, since the BPs and separatrices associated with them are structurally stable features.

Our model suggests the following scenario for the formation of a prominence and subsequent development of a two-ribbon flare in twisted magnetic configurations (like those shown in Fig. 1). In the process of slow emergence of the flux tube from below the photosphere a dense plasma is captured and lifted up in corona due to a dip of the field lines beneath the flux tube. Such a process must occur in a narrow layer between the photosphere and corona. Its beginning corresponds to the first appearance of the BP and the associated separatrix surface. The field lines under this surface are rooted in the photosphere near this BP and so when their coronal parts move upward they must be stretched down by the photospheric heavy and dense plasma. This stretching implies the appearance of a locally strong current density and hence an enhancement of ohmic diffusion of the captured material, so one can expect that during this process a part of it is left in the photosphere, while the rest is lifted up into corona and observed as the corresponding rise of the prominence. With further emergence of the flux tube its toroidal field dominates over poloidal one near the central part of the BP, so the BP bifurcates by producing two separatrix surfaces, which intersect under the tube along the separator field line. It is an open question whether or not such a slow evolution of the configuration is able to form strong current layers at the separatrices and separator itself due to the above mentioned line-tying effect. However, it seems quite plausible that slow magnetic reconnection at the separatrices makes the emergence of the twisted flux tube easier (by both liberating partly line-tying constraints and dense plasma). On the other hand, such a quasi-static evolution is probably stable only within a certain range of parameters. By taking into account line-tying effect and considering only axisymmetric and quasi-static perturbations we have estimated the stability of our twisted configuration. It has been shown that the configuration becomes unstable when the radius of curvature of the tube is comparable in value with the size of the active region. Strong current layers must be formed as soon as the unstable height is reached and due to this instability an eruption of the tube and the attached prominence must be developed. The formation of strong current layers along the separator and separatrices during the dynamic rise of the flux tube implies the onset of magnetic reconnection accompanyed by a characteristic chain of physical processes: an acceleration of plasma particles, hydrodynamic flows, an excitation of plasma waves and anomalous resistivity (which enhances the thermal heating of plasma) and an evaporation of the chromospheric material due to the thermal fluxes from the region of reconnection. For an observer it looks like an appearance of two sets of X-ray loops formed by reconnected field lines. According to our model these two loops must be located close to the lower and upper separatrix surfaces (see Fig. 6). The first ones must form a compact and bright arcade, while the second ones must be less bright and wrapped around the flux tube typically with one turn. This difference in brightness is due to the difference in the lengths and volumes of the corresponding loops. In many cases only the lower ones are detected, but in some well observed events both sets of loops are present (see Fig. 1 and the details in Manoharan et al.1996).

The observed Hα ribbons must be formed according to this scenario at the chromospheric level near the photospheric traces of our separatrices, where the dense plasma is energized by the accelerated particles and thermal fluxes. This fact is confirmed for two-ribbon flares (Gorbachev & Somov 1988), as well as for confined flares (Mandrini et al.1995, Démoulin et al.1997), even if the magnetic field is determined in potential or linear force-free approximation. The proposed model extends this result to a much more complicated nonlinear force-free magnetic fields. In fact, the Hα ribbons with the shape of separatrices found here have often been reported for several prominence eruptions and flares (Martin, 1979; Zirin, 1988, p. 281, 345 and 365 and Moore et al.1995). As shown above, the curvature and position of the ribbons with respect to the photospheric inversion line may also give an estimation of how much an observed configuration is twisted.

Acknowledgements. We thank Lidia van Driel-Gesztelyi for the picture shown in Fig. 1. V.S. Titov is grateful to all the colleagues from the DASOP of Paris-Meudon observatory for the warm hospitality during his stay there. He gratefully acknowledges financial support from Paris Observatory and Volkswagen-Foundation.

Appendix A: estimation of parameters for the onset of eruption

As described in Sect. 2.1 the external force balance is determined by $F_q + F_I = 0$, where by definition F_q and F_I are $\boldsymbol{n}$-components of the corresponding forces (4) and (5). From these components after simple calculations one can derive the following relative variation of the force:

$$\frac{\delta F_q+\delta F_I}{F_I}=\frac{\delta I}{I}+\frac{\delta R}{R}\left[\frac{2R^2-L^2}{R^2+L^2}\right]+ [\ln(8R/a)-3/2+l_{\rm i}/2]^{-1}\left(\frac{\delta R}{R}-\frac{\delta a}{a}\right). \quad \text{(A1)}$$

Here the variation of major radius δR is assumed to be arbitrary, while the variations of current δI and minor radius δa can be expressed in terms of δR. The conservation of toroidal flux in the flux tube $B_\theta \pi a^2 \approx \mathrm{const}$ yields

$$\frac{\delta a}{a}=\frac{1}{2}\frac{\delta R}{R}. \quad \text{(A2)}$$

The variation of current can be determined from the line-tying condition, which implies in our case that $N_{\rm cor}=\mathrm{const}$, from where with the help of (7), (9) and conservation of toroidal flux in the tube one obtains

$$\frac{\delta I}{I}=-\frac{\delta R}{R}\left[1+\frac{d}{(R^2-d^2)^{1/2}\,\arccos(d/R)}\right]. \quad \text{(A3)}$$

Combining all the above formula, we arrive at

$$\frac{\delta F_q+\delta F_I}{F_I}=\frac{\delta R}{R}\left[\frac{R^2-2L^2}{R^2+L^2}- \frac{d\,(R^2-d^2)^{-1/2}}{\arccos(d/R)}+\frac{1/2}{\ln(8R/a)-3/2+l_{\rm i}/2}\right], \quad \text{(A4)}$$

which shows that the force variation becomes positive (directed upward in the apex of the flux tube) at $R \gtrsim \sqrt{2}L$.

References

Aly J.J., 1990, In: Dezsõ L. (ed.) The Dynamic Sun. Public. Debrecen Obs., p. 176
Aly J.J., Amari T., 1989, A&A 221, 287
Aulanier G., Démoulin P., 1998a, A&A 329, 1125
Aulanier G., Démoulin P., Schmieder B., Fang.C., Tang Y.H., 1998b, Solar Phys. 183, 369
Billinghurst M.N., Craig I.J.D., Sneyd A.D., 1993, A&A 279, 589
Bungey T.N., Titov V.S., Priest E.R., 1996, A&A 308, 233
Démoulin P., Hénoux J.C., Mandrini C.H., 1994, A&A 285, 1023
Démoulin P., Hénoux J.C., Priest E.R., Mandrini C.H., 1996a, A&A 308, 643
Démoulin P., Priest E.R., Lonie D.P., 1996b, JGR 101, A4, 7631
Démoulin P., Bagalá L.G., Mandrini C.H., Hénoux J.C., Rovira M.G., 1997, A&A 325, 305
Finn J.M., Lau Y.T., 1991, Phys. Fluids B3, 2675
Forbes T.G., Priest E.R., 1995, ApJ 446, 377
Gorbachev V.S., Somov B.V., 1988, Solar Phys. 117, 77
Isenberg P.A., Forbes T.G., Démoulin P., 1993, ApJ 417, 368
Karpen J.T., Antiochos S.K., DeVore C.R., 1990, ApJ 356, L67
Karpen J.T., Antiochos S.K., DeVore C.R., 1991, ApJ 382, 327
Lau Y.T., 1993, Solar Phys. 148, 301
Lau Y.T., Finn J.M., 1990, ApJ 350, 672
Leka K.D., Canfield R.C., McClymont A.N., van Driel-Gesztelyi L., 1996, ApJ 462, 547
Li J., Metcalf T.R., Canfield R.C., Wulser J.P., Kosugi T., 1997, ApJ 482, 490
Lin J., Forbes T.G., Isenberg P.A., Démoulin P., 1998, ApJ 504, 1006
Lites B.W., Low B.C., Martinez Pillet V., et al., 1995, ApJ 446, 877
Low B.C., 1987, ApJ 323, 358
Low B.C., 1992, A&A 253, 311
Low B.C., Wolfson R., 1988, ApJ 324, 574
Mandrini C.H., Démoulin P., Rovira M.G., de la Beaujardiére J.F., Hénoux J.C., 1995, A&A 303, 927
Manoharan P.K., van Driel-Gesztelyi L., Pick M., Démoulin P., 1996, ApJ 468, L73
Martin S.F., 1979, Solar Phys. 64, 165
Moore R.L., La Rosa T.N., Orwig L.E., 1995, ApJ 438, 985
Pevtsov A.A., Canfield R.C., Zirin H., 1996, ApJ 473, 533
Raadu M.A., Schmieder B., Mein N., Gesztelyi L., 1988, A&A 197, 289
Rompolt B., 1990, Hvar Obs. Bull. Vol. 14, 1, 37
Rust D.M., Kumar A., 1994, Solar Phys. 155, 69
Seehafer N., 1985, Solar Phys. 96, 307
Seehafer N., 1986, Solar Phys. 105, 223
Seehafer N., Staude J., 1980, Solar Phys.67, 121
Shafranov V.D., 1966, In: Reviews of Plasma Physics 2, Consultants Bureau, New York, p. 103
Syrovatskii S.I., 1981, ARA&A 19, 163
Titov V.S., Priest E.R., Démoulin P., 1993, A&A 276, 564
Titov V.S., Démoulin P., 1999, PASP Conf. Series 184, 76
Titov V.S., 1999, Topology and reconnection of magnetic fields in solar corona. Izvestiya Akademii Nauk, Ser. fiz., No. 8, in press (in Russian)
Van den Oord G.H.J. 1993, Proc. of COSPAR meeting. In: Advances in Space Research 13 (9), 143
Vekstein G.E., Priest E.R., 1992, ApJ 384, 333
Vekstein G.E., Priest E.R., Amari T., 1991, A&A 243, 492
Vršnak B., Ruždjak V., Rompolt B., 1991, Solar Phys. 136, 151
Wolfson R., 1989, ApJ 344, 471
Zirin H., 1988, Astrophysics of the Sun. Cambridge University Press
Zwingmann W., Schindler K., Birn J., 1985, Solar Phys. 99, 133

Note added in proof: Recenetly, we have investigated the appearance of quasi-separatrix layers (QSLs) in the considered model of twisted magnetic configuration by using the refined theory of QSLs (see the electronic preprint at the URL `http://xxx.lanl.gov/abs/astro-ph/9909392`). The obtained results suggest that the QSL has to appear in such configuration at $R \gtrsim 100\,$Mm, which approximately corresponds to the moment when the genuine separatrix surfaces caused by BPs disappear. This means that the magnetic reconnection in sigmoidal flares at large hights in corona is due to the presence of QSLs, while at small hights it is due to the line-tying effect in BPs.